AIMS Geosciences

AIMS Geosciences, 12(4): 998–1020.
DOI: 10.3934/geosci.2026038
Received: 15 June 2026
Revised: 31 July 2026
Accepted: 08 September 2026
Published: 20 October 2026

https://www.aimspress.com/journal/geosciences

Research article

Generalized shear strain characteristics and damage evolution laws of salt rock under triaxial low-frequency cyclic loading

Lan Huang[1,†], Mingxin Wang[1,†], Xin Liu[2], Hui Gao[1] and Hongfa Xu[1,*]

[1] School of Urban Renewal, Shanghai Zhongqiao Polytechnic University, Shanghai, China
[2] CSSC International Engineering Co., Ltd., Beijing, China

* **Correspondence:** Email: xuhongfa1@sina.com; Tel: +86 21 31616156

† Co-first authors

Abstract: This paper focuses on the key mechanical issues of the surrounding rock in salt cavern underground gas storage subjected to low-frequency fatigue loading during long-term injection and production cycles. An in-depth study was conducted on the generalized shear strain evolution characteristics and damage evolution laws of salt rock via triaxial cyclic loading tests under confining pressures of 7–14 MPa and loading frequencies of 0.04–0.09 Hz. Based on the above test datasets, the evolutionary law of generalized shear strain (γ) of salt rock with generalized shear stress, cyclic frequency (f), stress level, and number of cycles (N) was systematically analyzed. Test data were standardized using dimensionless parameters (upper shear stress level, R_{up}, stress level amplitude, a_q, and frequency, f). The research results indicated that the development of generalized shear strain in salt rock exhibits two distinct stages: *decelerating development* and *stable constant-rate development*. The upper stress level is the dominant factor controlling strain accumulation. Using composite functions $\gamma = \alpha(1-e^{-\lambda N}) + vN + \gamma_0$ as constitutive models, a nonlinear fitting analysis was conducted on the test curves of each salt rock specimen. Through multiple nonlinear regression, a quantitative relationship between the model parameters and R_{up}, a_q, and f was obtained, thereby constructing a generalized shear strain constitutive equation with predictive capabilities. By defining the comprehensive influence factor $\beta = R_{up}^{\ 6}(a_q + f)^{0.6}$, a simplified constitutive equation was further obtained. The damage variable (ω) was defined based on the shear modulus degradation, and its evolutionary law follows an exponential saturation form $\omega = a[1-\exp(-N/b)]$. Thus, the damage evolution equation

$\omega = \left[0.11 + 0.2e^{-300(\beta-0.34)^2}\right]\left(1 - e^{-\frac{N}{9}}\right)$ was established, enabling a quantitative assessment of the damage state. The constitutive and damage models established in this study can provide a theoretical basis for evaluating the long-term stability of the surrounding rock in salt cavern underground gas storage and compressed air energy storage under cyclic loading.

Keywords: salt rock; triaxial low-frequency cyclic loading; generalized shear strain; damage evolution; constitutive model

1. Introduction

The deformation of rock consists of both volumetric deformation and generalized shear deformation, with the latter playing a critical role in rock failure. Salt rock is widely regarded as an ideal medium for underground energy storage (such as natural gas, petroleum, and hydrogen) and geological disposal of nuclear waste due to its extremely low permeability and favorable creep properties. However, during reservoir operations, the surrounding rock undergoes prolonged exposure to low-frequency fatigue loads induced by injection-production cycles; the degradation of its mechanical properties directly impacts the long-term safety and operational lifespan of the reservoir. Therefore, in-depth research on the generalized shear deformation characteristics of salt rock holds significant practical importance for assessing the stability of gas storage reservoirs.

Scholars both domestically and internationally have conducted a series of studies on the mechanical response of salt rock under cyclic loading. However, most studies focused on uniaxial stress states or volumetric deformation characteristics. For example, Fuenkajorn et al. investigated the effects of cyclic loading on the strength and elastic modulus of salt rock [1], and Liu et al. analyzed the damage evolution patterns of salt rock through uniaxial tests [2]. Liang et al. [3] conducted mechanical tests on different types of salt rock under two types of uniaxial cyclic loading (i.e., periodic loading and periodic loading-unloading), analyzing the variation patterns of strength, elastic modulus, and stress–strain curves. Yang Chunhe et al. [4] conducted uniaxial cyclic loading and unloading tests on salt rock, analyzing the characteristics of loading and unloading curves, variation patterns of the modulus of deformation, and constitutive relationships during loading and unloading under simple stress conditions. Xu Hongfa et al. [5] systematically investigated the volumetric strain characteristics of salt rock under triaxial low-frequency cyclic loading and established a corresponding empirical constitutive model. However, the macroscopic failure of rock is often closely associated with the formation and development of shear deformation zones. The generalized shear strain is a key indicator characterizing the plastic deformation and failure process of rocks. For rock-soil materials such as salt rock, its deformation mechanism is complex, with ball stress and generalized shear stress exhibiting significant cross-effects on volumetric strain and generalized shear strain [6,7]. Therefore, focusing solely on volumetric deformation is insufficient to fully elucidate the failure mechanisms of salt rock; as such, research on the generalized shear strain characteristics and damage mechanisms is particularly important.

In recent years, scholars have made significant progress in the field of cyclic deformation and damage evolution in salt rock. Wang Junbao et al. [8–10] systematically elucidated the creep-fatigue

interaction mechanism of salt rock under low-frequency triangular and trapezoidal wave loads and established a nonlinear constitutive model that considers irreversible deformation and elastic modulus degradation. Among their series of works, Wang et al. (2022) [9] adopted mercury intrusion porosimetry and SEM tests to reveal the coupling relationship between micropore structural variation and macroscopic cyclic damage, developing a microscopically driven damage evolution model via multi-stage fatigue tests with different upper stress limits. On this basis, Wang et al. (2024) [10] further introduced CT scanning to quantitatively track real-time pore evolution during cyclic loading and proposed a porosity-dependent constitutive model to describe the full fatigue damage process. These two representative studies construct a complete micro–macro linkage framework for salt rock cyclic damage analysis. The microstructural damage mechanism summarized by Wang's team provides essential physical interpretation for the decelerating and stable strain stages captured in this work, which strongly supports the rationality of the damage evolution law derived in our research.

Apart from microscale pore evolution analysis, some researchers have focused on the deformation response of salt rock under variable boundary confining pressure. Fan Jinyang et al. [11] investigated salt rock deformation under cyclic confining pressure, revealing that both the upper and lower limits of confining pressure, together with axial force, influence residual strain accumulation and elastic recovery. Their research elucidated the mechanism of plastic shrinkage under complex stress paths. Regarding damage evolution, Zhang Qiang [12] characterized cyclic damage by pore expansion via nuclear magnetic resonance and SEM observations and further established a fatigue damage equation based on microscopic pore evolution features.

A large number of studies adopted acoustic emission monitoring to capture the real-time damage signal of salt rock under multi-level cyclic loading. Li Zongze et al. [13] analyzed the damage evolution rules of salt rock under multi-stage amplitude creep-fatigue loading with acoustic emission equipment. Similarly, Zhao Kai et al. [14] and Li Hang et al. [15] separately explored the deformation and acoustic emission response characteristics under graded cyclic loading and multi-stage cyclic loading, which jointly improve the theoretical system of salt rock fatigue damage identification.

To evaluate the damage state from an energy perspective, Dai Jingjing et al. [16] pointed out that increased deviatoric stress significantly raises the elastic energy and energy dissipation rate of salt rock; both the elastic and dissipated energy of deep salt rock show a two-stage growth trend during cyclic loading and unloading. On this basis, Hao Lin et al. [17] clarified the intrinsic correlation between cyclic damage characteristics and internal energy evolution, providing a new quantitative evaluation route for salt rock damage degree.

In the past two years, several frontier studies further supplemented creep-fatigue constitutive models oriented to actual salt cavern operation conditions: Li et al. [18] carried out long-term discontinuous creep-fatigue tests matching the peak-shaving working condition of compressed air energy storage caverns and constructed a creep-fatigue coupling constitutive model with hardening state variables and unloading crack factors to quantify the memory effect of historical cyclic paths on viscoplastic strain. Wang Z. et al. [19] conducted triaxial multi-stage thermo-creep tests with real-time acoustic emission monitoring for deep salt rock. Their results proved that temperature elevation accelerates steady creep rate and alters the generation mode of intergranular and intragranular microcracks under thermo-mechanical coupling conditions. He et al. [20] performed complex cyclic fatigue tests on Jintan salt rock considering stress holding periods. They quantified the weight of each loading factor on accumulated shear strain by machine learning and put forward a

composite fatigue-creep damage model applicable to variable stress and dwell-time paths of underground gas storage.

Overall, existing investigations have systematically explored cyclic damage behaviors of salt rock from multiple perspectives, including micropore structural evolution, cyclic confining pressure effects, acoustic emission monitoring, and energy dissipation mechanisms, and a series of creep-fatigue constitutive models have been established for diverse loading conditions. Nevertheless, most existing models adopt microscopic pore parameters or energy dissipation as core state variables, while few works systematically describe the full-range evolution of generalized shear strain under triaxial low-frequency cyclic loading. Despite abundant research on volumetric deformation and partial damage mechanisms, quantitative constitutive characterization of shear strain accumulation and coupled shear damage deterioration remains insufficient, restricting comprehensive recognition of salt rock fatigue evolution.

It should be clearly emphasized that all triaxial low-frequency cyclic loading experimental data adopted in this paper are fully sourced from the test database published in the authors' previous study [5], which only targeted the volumetric strain characteristics of salt rock under cyclic loading and constructed an empirical constitutive model for volumetric deformation, while the macroscopic shear plastic deformation and fatigue damage evolution of salt rock were not considered. Based on this research gap, this paper focuses on investigating the coupling effects of generalized shear stress, upper stress level, cyclic number, and stress amplitude on generalized shear strain. Using the existing triaxial cyclic loading test data from [5], this study constructs a quantitative constitutive equation describing generalized shear strain evolution via dimensionless normalization and multivariate nonlinear regression. Furthermore, a shear modulus degradation-based damage variable is defined, and an exponential saturation damage evolution model correlated with a comprehensive influence factor is established, which can provide a novel theoretical reference for the long-term stability analysis of salt rock underground gas storage facilities.

2. Experimental design and results

All experimental raw data adopted in the present paper originate from the triaxial low-frequency cyclic loading tests of Qianjiang salt rock published by the authors in [5]. No additional laboratory tests, specimen processing, or loading schemes were carried out in this work. In [5], volumetric strain was the research object, revealing volumetric deformation rules under cyclic loading, whereas this paper reprocesses the original axial and radial strain data from the same batch of tests to calculate generalized shear strain, further analyzing shear deformation accumulation and cyclic damage degradation characteristics. To facilitate the subsequent analysis of generalized shear strain and damage evolution, this section briefly reorganizes the specimen preparation, test equipment, loading schemes, and dimensionless parameter definition from [5].

2.1. Specimen preparation and physical parameters

The rock cores used in the experiment were obtained from the Qianjiang Salt Mine in Hubei Province through core sampling via drilling and casing. Due to the brittle nature and high water solubility of salt rock, saturated brine is used throughout the sampling and processing procedures as a

cooling and lubricating medium to ensure the physical and chemical integrity of the specimens. After precision machining on a CNC lathe, the specimens were prepared into cylindrical shapes conforming to the International Society for Rock Mechanics (ISRM) recommended standards, with a height-to-diameter ratio of approximately 2:1. The nominal dimensions were Φ 50 mm × 100 mm, with actual dimensional tolerances controlled within ±3 mm.

The basic physical parameters of the eight processed salt rock specimens are shown in Table 1. The specimen's primary mineral composition consists of NaCl, with minor amounts of Na_2SO_4, $CaSO_4$, and clayey impurities. Its appearance exhibits varying shades of grayish-black. As shown in Table 1, the density of most specimens is around 2100 kg/m³, with only Specimen No. 4 exhibiting a significantly higher density. This is presumed to be related to the impurity composition and content present in the specimen. We have reexamined the generalized shear stress–strain hysteresis curves, cumulative shear strain evolution, and shear modulus degradation curves of Specimen No. 4, and found no significant deviation in its macroscopic mechanical behavior compared to other groups. Therefore, this specimen was included in the unified regression analysis to avoid bias caused by subjective screening and artificial data exclusion.

Table 1. Physical and geometric parameters of salt rock specimens.

Specimen number	Diameter (mm)	Height (mm)	Quality (g)	Density (kg·m^{-3})
1	52.22	101.91	460.59	2111.32
2	51.83	102.15	455.54	2114.74
3	54.61	105.49	519.06	2101.80
4	52.57	101.72	580.57	2630.89
5	50.20	103.74	426.97	2080.53
6	51.23	102.12	448.55	2131.97
7	50.06	102.77	441.05	2181.57
8	49.88	102.49	426.01	2128.22

2.2. Test equipment and loading procedure

The tests were conducted on a TAW-2000 microcomputer-controlled electro-hydraulic servo rock triaxial testing machine. The system can independently and precisely control axial pressure and confining pressure while collecting stress, axial strain, and radial strain data in real time.

The test first applied a predefined confining pressure (7 or 14 MPa) at a rate of 0.002 kN/s and maintained it constant, followed by the application of a low-frequency sinusoidal cyclic axial load. Loading commences with cyclic testing and continues until specimen failure or cumulative loading time exceeds 3 h, after which it transitions to monotonic loading until failure. The specific loading frequency (f), axial stress upper and lower limits (σ_{1max}, σ_{1min}), and confining pressure (σ_3) are detailed in Table 2. The experimental schemes (Table 2) aims to investigate the effects of varying confining pressures, stress levels, and loading frequencies on the mechanical behavior of salt rock.

Table 2. Experiment schemes (Xu, et.al. 2015) [5].

Specimen number	F (Hz)	σ_1		σ_3 (MPa)
		σ_{1max} (MPa)	σ_{1min} (MPa)	
1	0.083	28.881	26.987	7
2	0.083	27.245	23.741	7
3	0.050	24.831	17.018	7
4	0.056	26.507	12.209	7
5	0.050	38.861	20.220	14
6	0.071	29.578	17.862	14
7	0.043	40.435	19.874	14
8	0.042	38.871	17.144	14

2.3. Definition of dimensionless parameters

To eliminate the influence of individual specimen variations and enable universal analysis, this study introduced dimensionless parameters. Under triaxial stress conditions ($\sigma_1 \neq \sigma_2 = \sigma_3$), the generalized shear stress (q) and spherical stress (p) can be calculated using the following formula [21]:

$$q = \frac{1}{\sqrt{2}}\sqrt{(\sigma_1-\sigma_2)^2+(\sigma_2-\sigma_3)^2+(\sigma_3-\sigma_1)^2} = \sigma_1-\sigma_3 \tag{1}$$

$$p = \frac{1}{3}(\sigma_1+\sigma_2+\sigma_3) = \frac{1}{3}(\sigma_1+2\sigma_3) \tag{2}$$

The generalized shear strain (γ) is calculated from the strain components according to the following formula [21]:

$$\gamma = \frac{\sqrt{2}}{3}\sqrt{(\varepsilon_1-\varepsilon_2)^2+(\varepsilon_2-\varepsilon_3)^2+(\varepsilon_3-\varepsilon_1)^2} = \frac{2}{3}(\varepsilon_1-\varepsilon_3) \tag{3}$$

Based on the above definition, three key dimensionless parameters are further introduced to analyze their influence on the generalized shear strain:

• Upper limit shear stress level (R_{up}): Defined as the ratio of the maximum generalized shear stress (q_{max}) in the cycle to the generalized shear strength of the salt rock (q_s). It reflects the relative magnitude of the load.

$$R_{up} = \frac{q_{max}}{q_s} \tag{4}$$

• Stress level amplitude (a_q): Defined as the ratio of the amplitude to the strength on generalized shear stress, it quantifies the fluctuation amplitude of the generalized shear stress.

$$a_q = \frac{q_{\max} - q_{\min}}{q_s} \tag{5}$$

• Load frequency (f): The frequency of axial cyclic loading.

In the above formula, the generalized shear stress strength (q_s) is derived based on the axial peak strength of salt rock as determined in [5], namely:

$$q_s = 1.001\sigma_3 + 15.739 \ \text{(MPa)} \tag{6}$$

According to equation (6), the generalized shear stress strengths of the salt rock specimens under confining pressures of 7 and 14 MPa are calculated to be 22.746 and 29.753 MPa, respectively.

The test parameters in Table 2 are non-dimensionalized to obtain the dimensionless parameters shown in Table 3. Given that the test conditions for Sample No. 1 and Sample No. 2 are nearly identical, and taking into account the inherent compositional variations in the salt rock specimens, the data from these two samples are averaged and collectively denoted as "1–2".

Table 3. Experimental dimensionless parameters.

Number	q_{max}~q_{min} (MPa)	q_s (MPa)	R_{up}	a_q	f (Hz)
1	21.881~19.987	22.746	0.962	0.083	1/12
2	20.245~16.741	22.746	0.890	0.154	1/12
1-2	21.063~18.364	22.746	0.926	0.119	1/12
3	17.831~10.018	22.746	0.784	0.344	1/20
4	19.584~5.168	22.746	0.861	0.634	1/18
5	24.861~6.22	29.753	0.836	0.627	1/20
6	15.578~3.862	29.753	0.524	0.394	1/14
7	26.539~5.867	29.753	0.889	0.692	1/23
8	24.871~3.144	29.753	0.836	0.730	1/24

The above dimensionless parameter system provides a foundation for subsequently constructing a generalized shear strain constitutive model and damage evolution equation.

2.4. Test results

Based on the stress–strain curve test results from [5], data are transformed using generalized shear stress (q) and generalized shear strain (γ) to obtain the test curve shown in Figure 1.

In this cyclic test, due to experimental constraints, the salt rock specimen did not reach the failure stage. Therefore, two main phases of shear deformation were observed: first, the initial elastic phase where shear deformation developed rapidly; second, the subsequent stable cyclic phase where shear plastic deformation progressed slowly and exhibited a continuous accumulation trend.

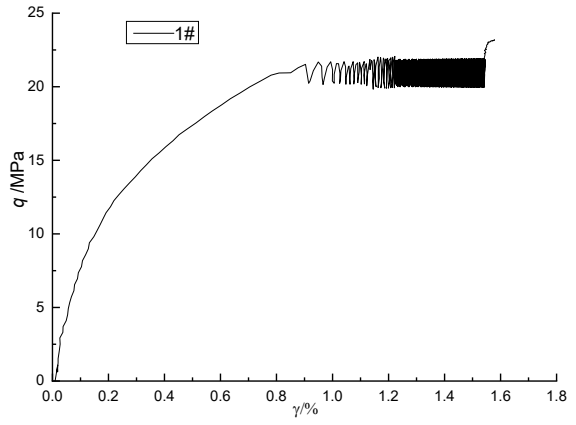

(a) Specimen No. 1

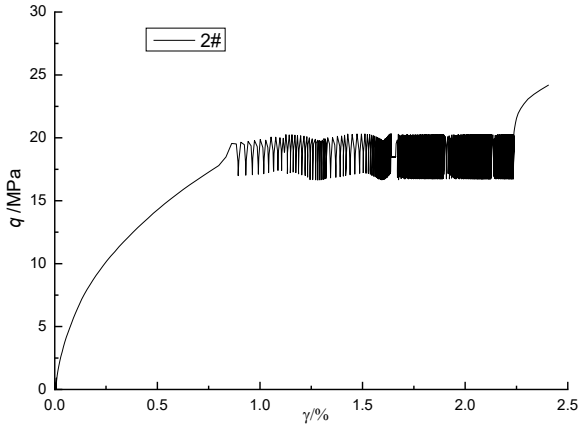

(b) Specimen No. 2

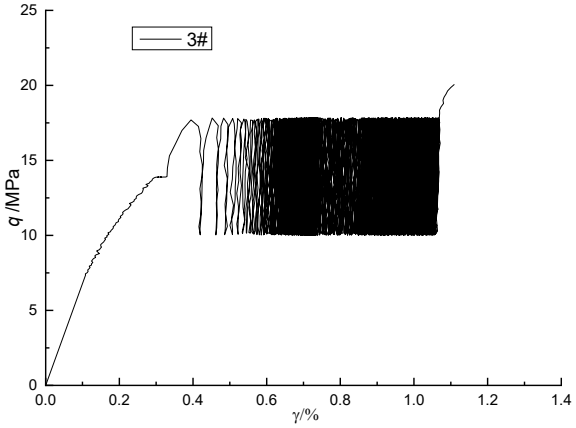

(c) Specimen No. 3

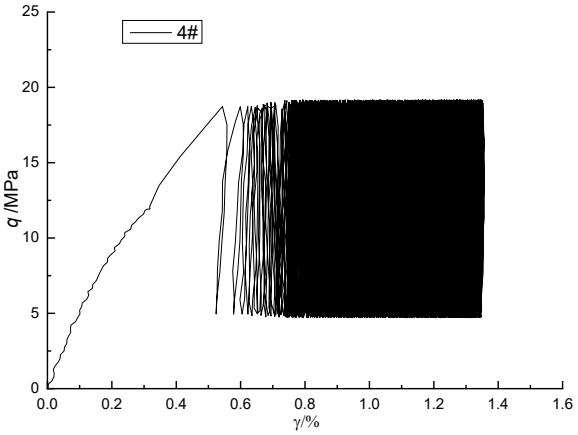

(d) Specimen No. 4

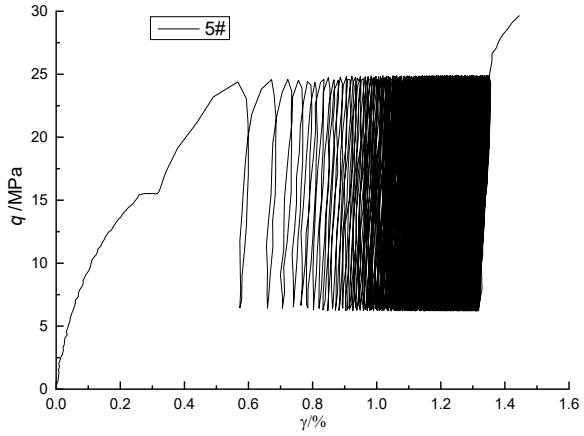

(e) Specimen No. 5

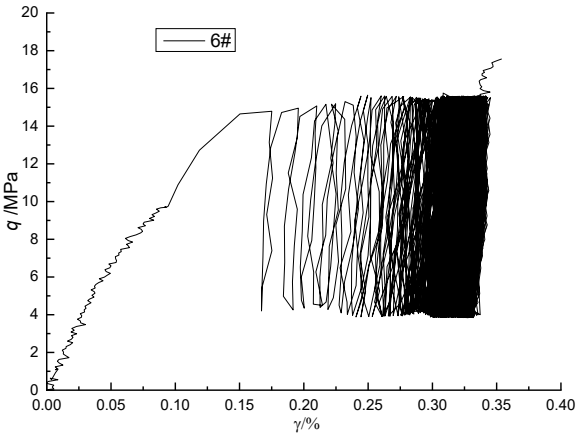

(f) Specimen No. 6

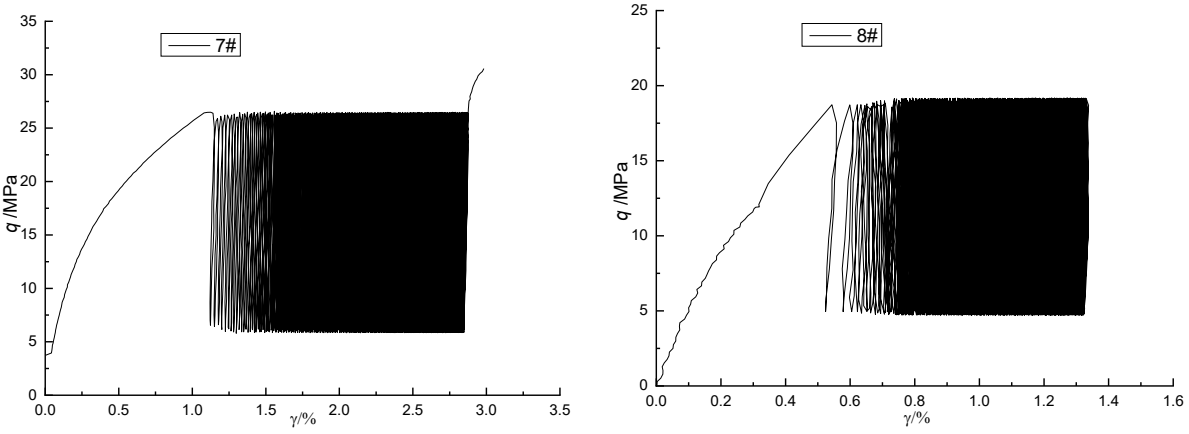

(g) Specimen No. 7 (h) Specimen No. 8

Figure 1. Curves of generalized shear stress-generalized strain.

3. Analysis of generalized shear strain characteristics

Based on the experimental scheme, dimensionless parameters, and test results above, this section conducts an in-depth analysis of the generalized shear strain characteristics of salt rock under cyclic loading. First, it clarifies the macroscopic mechanical response characteristics, then reveals their development laws with the number of cycles, and finally establishes a constitutive model that can quantitatively describe this process.

3.1. Characteristics of the generalized shear stress–strain curves

Stress–strain data obtained from the tests were converted into a generalized shear stress (q)-generalized shear strain (γ) relationship using Equations (1) and (3), with the results shown in Figure 1. The q–γ curves of all specimens exhibited typical cyclic loading and unloading characteristics. Observing Figure 1, it can be seen that the macro-level pattern of the curve is primarily composed of two phases, with the following key characteristics:

• Initial elastic stage: During the initial loading process, the generalized shear stress–strain curve exhibits a linear increase, with strain rapidly rising with stress, primarily manifesting as recoverable elastic deformation.

• Cyclic plastic accumulation stage: After entering the cycle, the q–γ curve forms a hysteresis loop. As the number of cycles N increases, the hysteresis loop continuously shifts to the right, indicating that the generalized shear strain accumulates with the number of cycles, resulting in irreversible plastic deformation.

• The hysteresis loop is sparse at first and then dense: Within the preset load levels and limited number of cycles in the test, the hysteresis loops gradually shifts less to the right, with the curves showing a sparse-then-dense pattern. In the later stages, the shape, position, and area of the hysteresis loops show no significant changes, indicating that the shear deformation of the salt rock has entered a relatively stable development phase.

• The cyclic loading test does not enter the accelerated failure stage.

3.2. Relationship between shear strain and number of cycles

To further quantify the development laws of generalized shear strain, a relationship curve between generalized shear strain (γ) and number of cycles (N) was plotted, as shown in Figure 2. Analysis of Figure 2 reveals the following laws:

• Two-stage evolutionary characteristics: The development of generalized shear strain can be clearly divided into two stages. In the initial deceleration stage, during the early part of the cycle, the rate of increase in generalized shear strain is relatively rapid but gradually slows down as the number of cycles increases. In the stable constant-rate development stage, subsequently, the strain growth rate stabilizes, with the generalized shear strain exhibiting an approximately linear relationship with the number of cycles. Due to the limited duration of the test, no accelerated failure stage was observed.

• Influence of test conditions: The strain accumulation rates and final strain values of different specimens exhibit significant differences. For example, Specimen 7 exhibited significantly higher cumulative strain rate and total strain compared to other specimens due to its elevated upper stress level (R_{up} = 0.889) and stress amplitude (a_q = 0.692). In contrast, Specimen 6 exhibited the lowest upper stress level (R_{up}= 0.524) and extremely slow strain development. This preliminary finding indicates that the upper stress level is the key factor governing the development of generalized shear strain.

• Outlier handling: The strain rate of Specimen No.3 changed after approximately 550 cycles. To ensure consistency in the analysis, only data from the first 550 cycles were used in subsequent modeling.

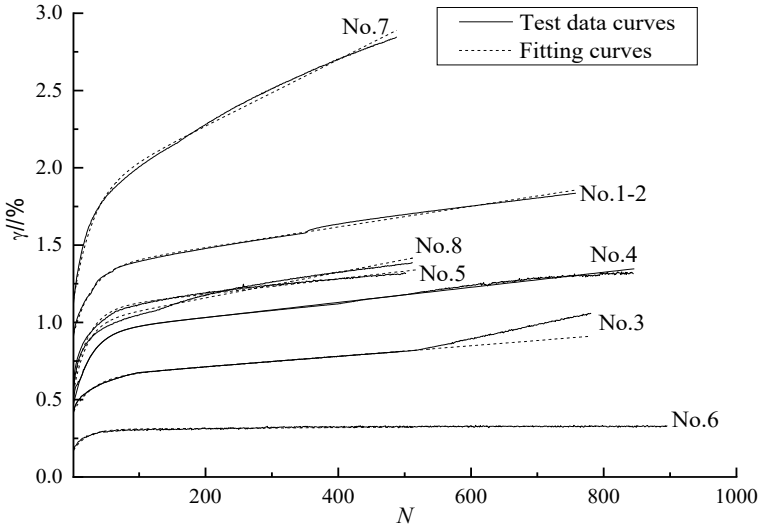

Figure 2. Generalized shear strain cyclic time curves.

3.3. Constitutive model establishment and parameter estimation

3.3.1. Constitutive model

To quantitatively describe the relationship between generalized shear strain and cycle times, a composite function incorporating an exponential decay term and a linear term is introduced as the constitutive model [22]:

$$\gamma = \alpha(1 - e^{-\lambda N}) + vN + \gamma_0 \tag{7}$$

where α is the exponential term amplitude parameter, reflecting the strain potential during the deceleration development stage; v is the linear term rate parameter that controls the strain rate during the stable development phase; λ is the decay coefficient for the exponential term, describing the rate of transition from the deceleration phase to the steady state; and γ_0 is the initial generalized shear strain. The physical meaning of Eq. (7) and each model parameter and its connection with salt rock microstructural evolution are as follows: γ_0 is the initial instantaneous shear strain from the first cyclic load; α reflects the maximum plastic deformation induced by early rapid microcrack initiation and grain slip; λ controls how fast the deformation shifts from deceleration to stable stage; and v stands for the steady plastic sliding rate of mineral grains in the later cyclic phase. The exponential term describes fast decaying micro-damage growth at early cycles, while the linear term characterizes stable long-term shear accumulation, matching the two-stage deformation observed in tests. Compared with existing creep-fatigue models, where most models take time as the core variable and focus on creep behavior, this model uses cycle number N to fit periodic injection-production conditions of salt caverns. Different from pore/energy-based microscopic fatigue models, this work builds a macroscopic constitutive framework centered on generalized shear strain, which provides a complementary macroscopic description for salt rock cyclic deformation analysis.

Nonlinear fitting was performed on the test data of each specimen using Equation (7), and the results of each parameter are shown in Table 4. The fitted curves show good agreement with the experimental data, with coefficients of determination (R^2) all above 0.94, demonstrating that the model can effectively describe the generalized shear strain evolution process of salt rock.

Table 4. Fitting parameters for generalized shear strain cycle times.

Specimen number	α	v	λ	γ_0 / %	R^2
1–2	0.41893	0.000665	0.03288	0.9327	0.99645
3	0.16396	0.000516	0.04965	0.43243	0.96137
4	0.45029	0.000486	0.0372	0.4848	0.99686
5	0.42919	0.000462	0.03209	0.66661	0.99487
6	0.12239	0.000025	0.04014	0.1873	0.94372
7	0.70309	0.000221	0.03892	1.12207	0.99627
8	0.37887	0.000800	0.03662	0.62397	0.98805

Considering that λ in Table 4 varies slightly between 0.03209 and 0.04965, to simplify the model, λ is fixed at the average value of 0.04 from the fitted values of each specimen. The refitted parameters are shown in Table 5. The refitted curves (see Figure 2) all have a coefficient of determination (R^2) above 0.94 when fitted to the experimental data, indicating that this simplification is reasonable.

Table 5. Refitted parameters of generalized shear strain cyclic times.

Specimen number	α	v	λ	γ_0/%	R^2
1–2	0.44789	0.000679	0.04	0.89663	0.99584
3	0.14648	0.000513	0.04	0.45156	0.96052
4	0.46287	0.000490	0.04	0.4700	0.99672
5	0.45358	0.000498	0.04	0.62902	0.99294
6	0.12222	0.000025	0.04	0.1875	0.94378
7	0.70784	0.0022	0.04	1.11481	0.99614
8	0.38773	0.000811	0.04	0.61088	0.97842

To quantify the influence of fixing $\lambda = 0.04$ on model prediction accuracy and verify the robustness of this parameter simplification, a series of global nonlinear fittings with fixed λ values ranging from 0.01 to 0.07 were performed via Origin software. Three evaluation indicators, namely mean R^2, average maximum relative prediction error (MRPE), and average root mean square error (RMSE), were calculated for all specimens, and the full statistical results are summarized in Table 6.

Table 6. Sensitivity analysis statistical results of parameter λ.

λ	Mean R^2	Average MRPE (%)	Average RMSE
0.01	0.9527	39.2644	0.02445
0.02	0.9739	26.2905	0.01705
0.03	0.9811	16.6645	0.01392
0.04	0.9819	9.6245	0.01441
0.05	0.9795	7.4387	0.01649
0.06	0.9756	7.5351	0.01878
0.07	0.9710	8.9202	0.02091

Note: MRPE is the maximum relative error $|\gamma_{\text{pred}} - \gamma_{\text{exp}}|/\gamma_{\text{exp}} \times 100\%$ of all measuring points of all specimens. Root mean square error (RMSE) directly reflects the absolute deviation between the predicted strain and test data.

From the statistical results in Table 6, the following rules can be drawn:

• The mean R^2 reaches its maximum value of 0.9819 at $\lambda = 0.04$, which is the fixed value adopted in this paper. When λ varies within the range of 0.03–0.05, the mean R^2 remains higher than 0.9795, showing excellent overall fitting performance.

• The average MRPE is only 9.62% at $\lambda = 0.04$. Within the concentrated interval $\lambda = 0.03$–0.05, the average MRPE is controlled below 16.67%. When λ deviates severely to 0.01 or 0.02, the average MRPE rises sharply to 39.26% and 26.29%, and the model prediction accuracy decreases significantly.

• The average RMSE reaches the minimum value of 0.01392 at $\lambda = 0.03$ and remains at a low level of 0.01441 at $\lambda = 0.04$. The absolute prediction deviation only increases obviously when λ is less than 0.02 or larger than 0.06.

All freely fitted λ values of the experimental specimens are distributed between 0.0321 and 0.0497, which is fully covered by the high-precision interval $\lambda = 0.03$–0.05. The fitting accuracy loss

and prediction error introduced by fixing λ = 0.04 are limited and acceptable for engineering long-term stability evaluation of salt rock gas storage caverns.

The above sensitivity analysis fully verifies the robustness and rationality of fixing λ=0.04 to simplify the constitutive model.

3.3.2. Parameter estimation

To establish a constitutive equation with predictive capability, the model parameters (α, v, γ_0) must be correlated with the dimensionless influencing factors (R_{up}, a_q, f).

• Estimation of parameter γ_0: γ_0 is the initial generalized shear strain, primarily dependent on the upper stress level R_{up} associated with the initial loading state.

According to the γ_0 and R_{up} data in Table 5, a nonlinear fitting is performed, and the fitting curve is shown in Figure 3. The relationship between γ_0 and Rup is obtained as:

$$\gamma_0 = \frac{R_{up}}{5.56 - 5R_{up}} \quad (R^2 = 0.71642) \tag{8}$$

Where γ_0 is the initial generalized shear strain (%).

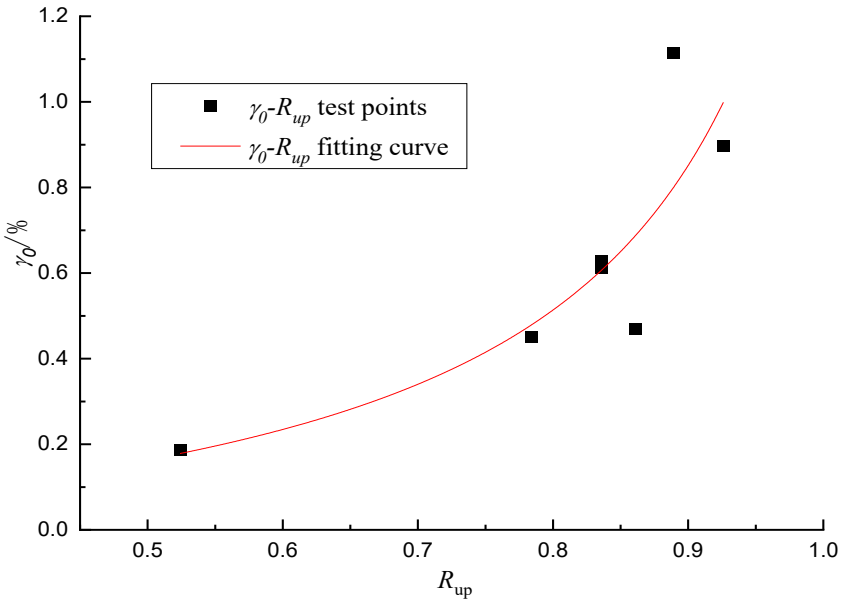

Figure 3. γ_0 - R_{up} fitting curve.

• Estimation of parameters α and $\boldsymbol{v}$: The parameters α and $\boldsymbol{v}$ are influenced by multiple factors, both being affected by R_{up}, a_q, and f. Performing multivariate nonlinear regression on Table 3 using a power function form yields:

$$\alpha = 10^{-2.8128} R_{up}^{1.8718} a_q^{3.2364} f^{0.0241} \quad (R^2 = 0.81329) \tag{9}$$

$$v = 10^{-4.3794} R_{up}^{1.2782} a_q^{7.0742} f^{0.2453} \quad (R^2 = 0.91858) \tag{10}$$

• Generalized shear strain constitutive model

By substituting equations (9) and (10) into equation (7), the generalized shear strain constitutive model (γ-N) of salt rock, considering the effects of stress level and frequency, is obtained as Equation (11). This model can be used to predict the evolution of the generalized shear strain of salt rock with cycle number under specified loading conditions.

$$\gamma = 10^{-2.8128} R_{up}^{1.8718} a_q^{3.2364} f^{0.0241} (1 - e^{-0.04N}) + 10^{-4.3794} R_{up}^{1.2782} a_q^{7.0742} f^{0.2453} N + \gamma_0 \tag{11}$$

3.3.3. Comprehensive impact factor β analysis

Given that the expression of the generalized shear strain constitutive model in Equation (11) is relatively cumbersome, the authors have identified a comprehensive influencing factor β through extensive computational analyses. Herein, the comprehensive influencing factor β is defined as follows:

$$\beta = R_{up}{}^{6} (a_q + f)^{0.6} \tag{12}$$

R_{up}, a_{q}, and f are all dimensionless loading parameters, so their combined term β remains dimensionless without dimensional conflict. The form of β is obtained through repeated traversal fitting: we tested multiple combination forms of power product and polynomial, and this specific expression achieves the highest correlation with model parameters α and ν simultaneously. Physically, β synthetically characterizes the overall excitation intensity of cyclic load on salt rock shear deformation, integrating the joint effect of upper stress level, stress amplitude, and loading frequency.

The relationship between the comprehensive influencing factor β and parameters α and v were obtained through calculations, as shown in Table 7.

Table 7. Relationship with parameters α and ν.

Specimen number	β	α	v (E–4)
1–2	0.24148	0.44789	6.79
3	0.1328	0.14648	5.13
4	0.32608	0.46287	4.90
5	0.27014	0.45358	4.98
6	0.01308	0.12222	0.25
7	0.41038	0.70784	22.00
8	0.29229	0.38773	8.11

Further analysis reveals that the comprehensive influencing factor β and parameters α and ν exhibit a good correlation, as illustrated in Figures 4 and 5.

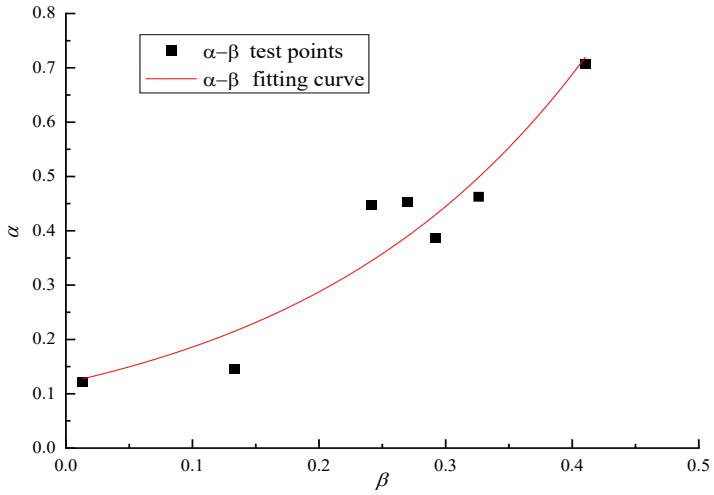

Figure 4. α-β fitting curve.

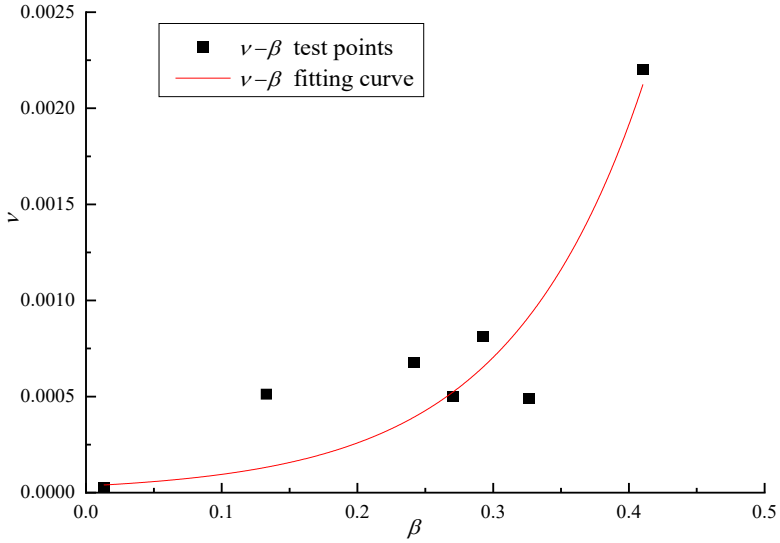

Figure 5. ν-β fitting curve.

Nonlinear fitting analysis was performed on the parameter relationships in Figures 4 and 5, and the corresponding expressions were obtained as follows:

$$\alpha = 0.12e^{4.36\beta} \quad \text{(Correlation coefficient } R^2\text{=0.90807)} \tag{13}$$

$$\nu = 3.5e^{10\beta} \times 10^{-5} \quad \text{(Correlation coefficient } R^2\text{=0.84452)} \tag{14}$$

Thus, by substituting Equations (13) and (14) into Equation (7), the simplified expression of the γ-N constitutive relation can be obtained as:

$$\gamma = 1.12e^{4.36\beta}(1-e^{-0.04N}) + 3.5e^{10\beta} \times 10^{-5} N + \gamma_0 \ \ (\%) \tag{15}$$

4. Shear modulus and cyclic damage analysis

The development of generalized shear deformation is closely related to the deterioration of the internal structure of salt rock, and the variation of shear modulus serves as a key indicator to characterize such deterioration. By analyzing the evolution pattern of shear modulus, this section defines and quantifies the damage variable under cyclic loading and further establishes the damage evolution model of salt rock. The fatigue damage mechanism of salt rock is revealed from the perspectives of energy dissipation and material softening.

4.1. Variation law of shear modulus

Based on the generalized Hooke's law [21], the shear modulus under triaxial stress state can be calculated by the slope of the elastic curve, and its expression is as follows:

$$G = \frac{\sigma_1 - \sigma_3}{2(\varepsilon_1 - \varepsilon_3)} = \frac{q}{3\gamma} \tag{16}$$

where G is the shear modulus. For each cycle, the maximum and minimum generalized shear stress and corresponding generalized shear strain of the hysteresis loop are extracted to calculate the cyclic secant shear modulus using Eq. (16). The variation curves of the shear modulus G with cycle number N for all specimens are plotted in Figure 6.

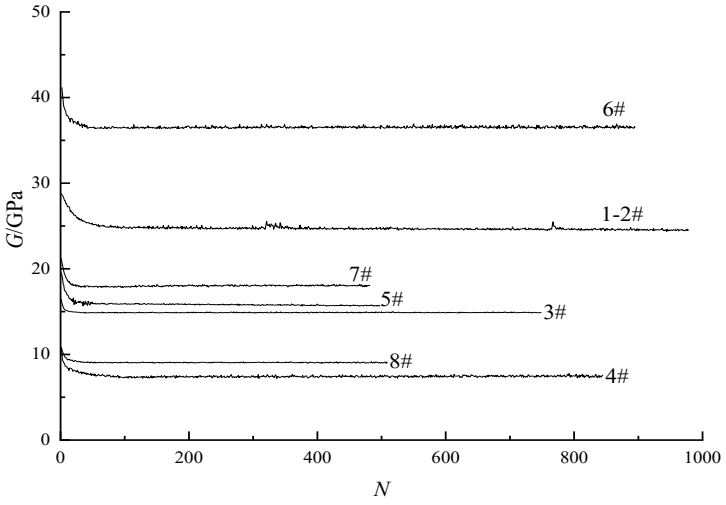

Figure 6. Relationship curves between shear modulus and number of cycles.

Analysis of Figure 6 reveals a consistent law: the shear modulus of all specimens exhibits a rapid attenuation trend in the initial stage of cycling, followed by a gradual slowing of the attenuation rate, finally tending to a stable residual value. This phenomenon indicates that the damage to the salt rock structure induced by cyclic loading is most significant in the initial stage, where defects such as microcracks and dislocations rapidly initiate and propagate, leading to a sharp decrease in the macroscopic mechanical parameter (shear modulus). As the cycles proceed, the material gradually achieves a new equilibrium adapted to the current stress state, and damage development tends to slow

down, thus resulting in the stabilization of the modulus. This law confirms the intrinsic mechanism of the two-stage "deceleration-stabilization" development of generalized shear strain presented above.

4.2. Definition of damage variable and evolution equation

To quantitatively describe the damage accumulation process of salt rock under cyclic loading, this paper adopts the modulus method to define the damage variable ω. This method directly characterizes damage through the degradation of material mechanical properties, defined as follows [23]:

$$\omega = 1 - \frac{G(N)}{G_0} \tag{17}$$

where ω is the damage variable; $G(N)$ is the shear modulus at the Nth cycle; and G_0 is the initial shear modulus. The initial shear modulus G_0 used to define damage variable is taken as the secant modulus of the first hysteresis loop. Note that, for specimens No. 1 and No. 2, due to the small load amplitude, no effective hysteresis loops were formed initially. The initial elastic modulus is calculated from the first effective hysteresis loop.

Under this definition, the range of ω is [0, 1]; when $\omega = 0$, the salt rock is undamaged; the larger the value of ω, the higher the degree of damage.

The damage variable ω of each specimen was calculated according to Equation (17), and its evolution curve with the number of cycles N is shown in Figure 7.

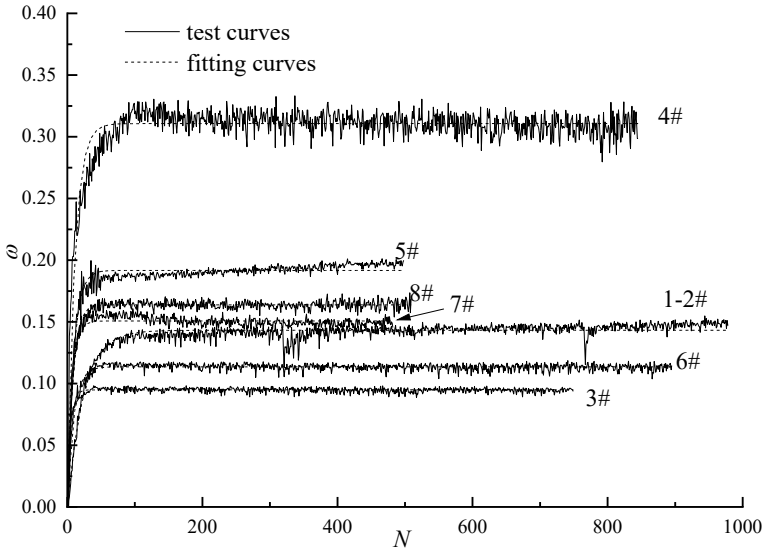

Figure 7. ω-N fitting curves.

The test results in Figure 7 show that the damage evolution also follows the laws of rapid initial development followed by stabilization. To describe this process, the following exponential function form of the evolution equation is used for fitting [24,25]:

$$\omega = a\left[1 - \exp\left(-\frac{N}{b}\right)\right] \tag{18}$$

Where parameter a represents the saturation value of the damage variable, which is the final stabilized level of damage; and parameter b represents the number of feature cycles, controlling the rate at which damage progresses toward saturation value. A smaller value of b indicates that the damage stabilizes more quickly.

Given the viscoelastic hysteresis characteristics of salt rock, the use of the hysteresis loop secant modulus instead of the elastic shear modulus is primarily based on two considerations. First, the secant line traverses the entire range of cyclic stress fluctuation, thereby effectively averaging the viscoelastic hysteresis deformation within the loop; second, adopting a unified calculation standard for all specimens ensures consistency in the modulus extraction rule under different confining pressures, stress amplitudes, and frequencies, thus enhancing the comparability of damage evolution curves across various loading conditions. Although this method simplifies the complex viscoelastic coupling process, it reliably characterizes the relative damage evolution trend of salt rock under cyclic loading, meeting the analytical requirements for long-term stability evaluation of salt cavern storage.

4.3. Damage model fitting and validation

Test data in Figure 7 (solid line) were fitted nonlinearly using Equation (18), and the results are shown in Table 8. The correlation coefficient R^2 for all fitted curves was higher than 0.79, indicating that this model can properly describe the trend of salt rock damage evolution.

Table 8. ω-N fitting parameters.

Number	a	b	R^2
1–2	0.14319	24.07294	0.92042
3	0.09477	5.05799	0.87764
4	0.31067	10.73087	0.79651
5	0.19166	9.27351	0.91598
6	0.11353	9.4409	0.85704
7	0.15071	7.03738	0.90582
8	0.16377	8.04143	0.92936

To simplify the model and enhance its engineering practicality, parameter b was standardized. After excluding the outlier (24.07) of Specimen 1–2, the average value of parameter b was 8.26; if the outlier is included, the average value of b would be 10.52. To simplify calculations, a fixed value of $b = 9$ was adopted based on comprehensive considerations. Substituting $b = 9$ into Equation (18), secondary fitting was conducted (see Figure 8), and the new parameter a was obtained (see Table 9). Comparative analysis revealed minimal differences in the fitted curve shapes before and after simplification, validating the rationality of the simplified approach.

Table 9. ω-N second fitting parameters.

Number	a	b	R^2
1-2	0.14126	9	0.658576
3	0.09507	9	0.703996
4	0.31019	9	0.786819
5	0.19158	9	0.915685
6	0.11349	9	0.855894
7	0.15115	9	0.868038
8	0.164	9	0.922936

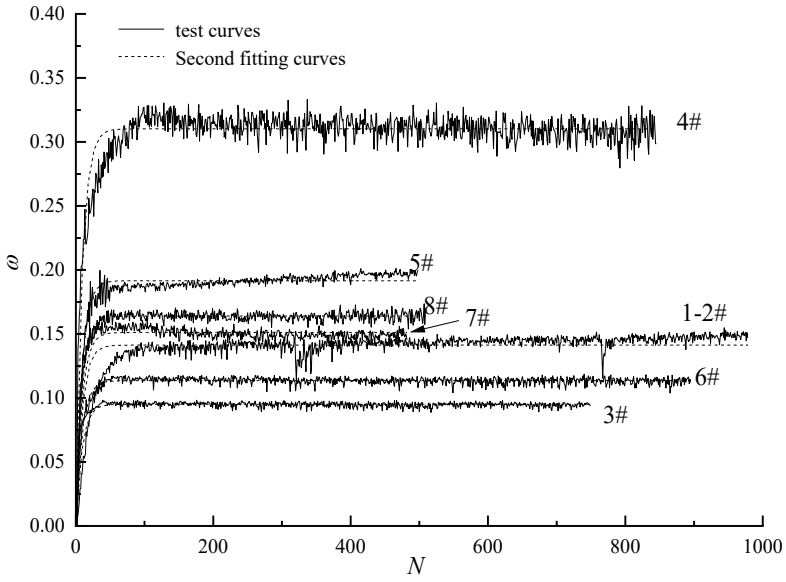

Figure 8. ω-N second fitting curves.

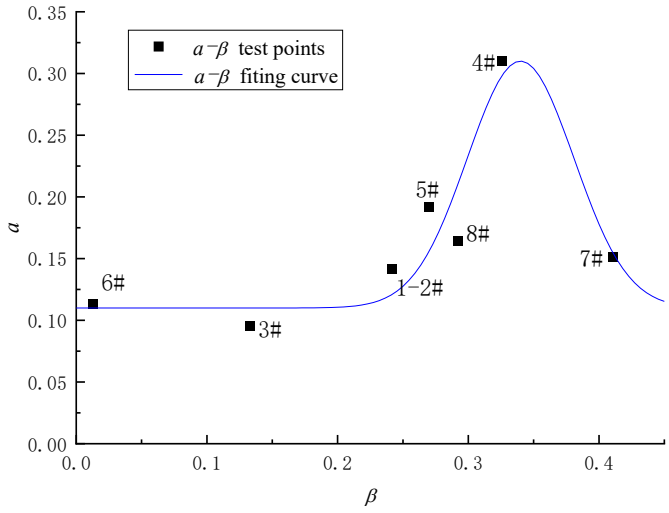

Figure 9. α-β fitting curves.

To predict damage based on external load conditions, the comprehensive influence factor β defined in Equation (12) is correlated with the damage saturation value a. A nonlinear fitting was performed using the data of a from Table 9 and β from Table 7 (see Figure 9), resulting in the empirical relationship:

$$a = 0.11 + 0.2e^{-300(\beta-0.34)^2} \quad \text{(Correlation coefficient } R^2=0.85872) \tag{19}$$

Thus, by substituting Equation (20) and the value b=9 into Equation (19), the evolution equation of the damage variable for salt rock under triaxial cyclic loading is obtained as follows:

$$\omega = \left[0.11 + 0.2e^{-300(\beta-0.34)^2}\right]\left(1 - e^{-\frac{N}{9}}\right) \tag{20}$$

This equation directly correlates macroscopic damage evolution to quantifiable load parameters (R_{up}, a_q,f), providing a theoretical tool for assessing the fatigue damage state of salt rock underground engineering under long-term cyclic loading.

5. Conclusions

This paper investigates the generalized shear strain evolution characteristics and damage mechanisms of salt rock through triaxial low-frequency cyclic loading tests, with the main conclusions being as follows:

• Generalized shear strain evolution law: The development of generalized shear strain for salt rock exhibits a typical two-stage characteristic: the initial deceleration stage and the subsequent stable constant-velocity stage. The upper limit stress level is the dominant factor controlling the strain accumulation rate and final amplitude, with its influence significantly higher than that of stress amplitude and loading frequency.

• Generalized shear strain constitutive model: Based on experimental data, a composite constitutive model capable of describing the entire evolution process of generalized shear strain was established as $\gamma = \alpha[1 - \exp(-\lambda N)] + \nu N + \gamma_0$. Through multivariate nonlinear regression, quantitative relationships between model parameters and dimensionless influencing factors (upper stress level, stress amplitude, frequency) were obtained, thereby constructing a predictive generalized shear strain constitutive equation. By defining a comprehensive influence factor β, a simplified constitutive model was derived.

• Damage evolution mechanism and model: The damage variable was defined based on the degradation of shear modulus, revealing that damage evolution follows a law of rapid initial progression followed by a slowdown and eventual saturation. By introducing a comprehensive influence factor β, a model was established that reflects loading conditions, enabling quantitative assessment of fatigue damage states in salt rock.

• Limitations of the study: The constitutive and damage models derived in this study are based on salt rock from a specific mining area and were applicable within a fixed confining pressure range (7~14 MPa) and low-frequency interval (0.04~0.09 Hz). The cross-validation analysis of model generalization performance will be systematically carried out in follow-up research with more abundant

test samples. The constitutive and damage equations proposed in this paper can provide a reference for relevant engineering analysis and subsequent theoretical research by peers. The established constitutive and damage evolution models are only valid for the pre-accelerated failure stable deformation stage. The general applicability to different geological conditions, higher confining pressures, or more complex loading paths (such as non-sinusoidal waves) requires further verification.

• Engineering significance and prospects: The research findings provide analytical methods for evaluating the stability of surrounding rock in salt rock underground gas storage and compressed air energy storage caverns in the long-term stable operation stage before accelerated damage occurs. Subsequent research can further explore temperature coupling effects and complex loading-unloading paths and combine microscopic testing means (mercury intrusion, SEM, nuclear magnetic resonance) proposed in Wang et al. [9] to carry out cross-scale research integrating macroscopic generalized shear deformation and microscopic pore damage evolution, so as to further improve the complete macro–micro coupled theoretical framework of salt rock fatigue failure under triaxial cyclic loading.

Author contributions

Hongfa Xu: conceptualization, methodology, validation, and writing—editing. Lan Huang: data curation, and writing—original draft preparation. Mingxin Wang: data curation, and writing—review. Xin Liu: validation, writing—review and editing. Hui Gao: formal analysis, and data curation. All authors have read and agreed to the published version of the manuscript.

Use of AI tools declaration

The authors declare they have not used Artificial Intelligence (AI) tools in the creation of this article except for text translation.

Acknowledgments

We would like to extend our sincere gratitude to the staff of the Rock Mechanics Laboratory at the University of Science and Technology Beijing for their equipment support. This work was supported by the 2025 Project of Shanghai Vocational Colleges 1 + X Certificate Special Committee (2025ZD01).

Conflict of interest

The authors declare that they have no known competing financial interests or personal relationships that could have appeared to influence the work reported in this paper.

References

1. Fuenkajorn K, Phueakphum D (2010) Effects of cyclic loading on mechanical properties of Maha Sarakham salt. *Eng Geol* 112: 43–52. https://doi.org/10.1016/j.enggeo.2010.01.002

2. Liu J, Xie H, Hou Z, et al. (2014) Damage evolution of rock salt under cyclic loading in uniaxial tests. *Acta Geotech* 9: 153–161. https://doi.org/10.1007/s11440-013-0236-5
3. Liang WG, Zhang CD, Gao HB, et al. (2012) Experiments on mechanical properties of salt rocks under cyclic loading. *J Rock Mech Geotech Eng* 4: 54–61. https://doi.org/10.3724/SP.J.1235.2012.00054
4. Yang CH, Ma HL, Liu JF (2009) Experimental Study on Deformation Characteristics of Salt Rock under Cyclic Loading and Unloading. *Rock Soil Mech* 30: 3562–3568. https://doi.org/10.16285/j.rsm.2009.12.027
5. Xu HF, Wang C, Ma LJ, et al. (2015) Study on the Volume Deformation Characteristics of Salt Rock under Triaxial Low-Frequency Cyclic Loading. *Chin J Geotech Eng* 37: 741–746. https://doi.org/10.11779/CJGE201504021
6. Chen CL, Xie DY, Gao P (2005) Experimental investigation on deformation characteristics of saturated sand under cyclic ball stress loading. *J Rock Mech Eng* 24: 513–520. https://doi.org/10.3321/j.issn:1000-6915.2005.03.025
7. Lu XL, Liu QS, Zhang W, et al. (2009) Experimental Study on Non-Elastic Volume Increase in Soft Rock under High Stress. *J Coal Sci Eng* 34: 903–906. https://doi.org/10.13225/j.cnki.jccs.2009.07.027
8. Wang JB, Zhang Q, Liu X, et al. (2025) *Mechanical Properties and Applications of Salt Rock under Cyclic Loading*, Science Press, Beijing. https://www.ecsponline.com/goods.php?id=232743
9. Wang JB, Zhang Q, Song ZP, et al. (2022) Microstructural variations and damage evolvement of salt rock under cyclic loading. *Int J Rock Mech Min* 152: 105078. https://doi.org/10.1016/j.ijrmms.2022.105078
10. Wang JB, Liu X, Zhang Q, et al. (2024) Fatigue Properties and Damage Constitutive Model of Salt Rock Based on CT Scanning. *Int J Min Sci Technol* 34: 245–259. https://doi.org/10.1016/j.ijmst.2024.01.002
11. Fan JY, Wu JT, Yang ZY, et al. (2025) Deformation Characteristics of Salt Rock Under Cyclic Confining Pressure. *J Saf Environ* 25: 1797–1804. https://doi.org/DOI:10.13637/j.issn.1009-6094.2024.1752
12. Zhang Q (2025) Creep-Fatigue Characteristics of Salt Rock Under Long-Term Cyclic Loading and Their Engineering Applications. *J Xi'an Univ Arch Tech.* https://doi.org/10.27393/d.cnki.gxazu.2021.001242
13. Li ZZ, Suo JJ, Fan JY, et al. (2023) Damage evolution of rock salt under multilevel amplitude creep–fatigue loading with acoustic emission monitoring. *Int J Rock Mech Min* 164: 105346. https://doi.org/10.1016/j.ijrmms.2023.105346
14. Zhao K, Ma HL, Li YP, et al. (2022) Deformation and damage evolution of rock salt under multilevel cyclic loading with constant stress intervals. *Eng Fract Mech* 260: 108191. https://doi.org/10.1016/j.engfracmech.2021.108191
15. Li H, Ma HL, Yang CH, et al. (2023) Acoustic emission characteristics of rock salt under multi-stage cyclic loading. *Int J Fatigue* 176: 107911. https://doi.org/10.1016/j.ijfatigue.2023.107911

16. Dai JJ, Liu JF, Ran L, et al. (2023) Acoustic Emission Characteristics and Energy Evolution of Engineering Salt Rock in Deep Salt Caverns under Triaxial Loading and Unloading Conditions. *J Cent South Univ* 30: 962–974. https://doi.org/10.1007/s11771-022-5213-4
17. Lin H, Liu JF, Yang JX, et al. (2022) Analysis of damage characteristics and energy evolution of salt rock under triaxial cyclic loading and unloading. *J Energy Storage* 56: 106145. https://doi.org/10.1016/j.est.2022.106145
18. Li ZZ, Fan JY, Fourmeau M, et al. (2024) Long-term deformation of rock salt under creep–fatigue stress loading paths: Modeling and prediction. *Int J Rock Mech Min* 181: 105861. https://doi.org/10.1016/j.ijrmms.2024.105861
19. Wang ZH, Chen F, Li HR, et al. (2025) Experimental Research on the Thermo-mechanical Damage Mechanisms of Salt Rock. *Rock Mech Rock Eng* 58: 4001–4021. https://doi.org/10.1007/s00603-024-04370-y
20. He QC, Liu JF, Wu F, et al. (2025) Fatigue properties and constitutive model of Jintan salt rock subjected to complex cyclic loading. *Int J Min Sci Technol* 35: 121–133. https://doi.org/10.1016/j.ijmst.2024.12.007
21. Molotnikov V, Molotnikova A (2021) *Theory of Elasticity and Plasticity: A Textbook of Solid Body Mechanics*, Springer Nature Switzerland AG. https://doi.org/10.1007/978-3-030-66622-4
22. Xu HF, Lu HB, Qian QH (2002) Creep damage effects on pulling grouting anchor in soil. *Chin J Geotech Eng* 24: 61–63. https://doi.org/10.3321/j.issn:1000-4548.2002.01.013
23. Lemaitre J (1996) *A course on damage mechanics*, Springer-Verlag Berlin Heidelberg. https://doi.org/10.1007/978-3-642-18255-6
24. Jaeger JC, Cook NGW, Zimmerman RW (2007) *Fundamentals of rock mechanics*, 4th ed., Wiley-Blackwell.
25. Liu JF, Xie HP, Hou ZM, et al. (2014) Damage evolution of rock salt under cyclic loading in uniaxial tests. *Acta Geotech* 9: 153–161. https://doi.org/10.1007/s11440-013-0236-5



AIMS Press

© 2026 the Author(s), licensee AIMS Press. This is an open access article distributed under the terms of the Creative Commons Attribution License (https://creativecommons.org/licenses/by/4.0)